ACS NANOSCIENCE Au
AN OPEN ACCESS JOURNAL OF THE AMERICAN CHEMICAL SOCIETY

pubs.acs.org/nanoau Letter

Spectrally Resolved Surface-Enhanced Raman Scattering Imaging Reveals Plasmon-Mediated Chemical Transformations

Carlos Diego L. de Albuquerque, Chelsea M. Zoltowski, Brian T. Scarpitti, Deben N. Shoup, and Zachary D. Schultz*

Cite This: *ACS Nanosci. Au* 2021, 1, 38–46 Read Online

ACCESS | Metrics & More | Article Recommendations | Supporting Information

ABSTRACT: Challenges investigating molecules on plasmonic nanostructures have limited understanding of these interactions. However, the chemically specific information in the surface-enhanced Raman scattering (SERS) spectrum can identify perturbations in the adsorbed molecules to provide insight relevant to applications in sensing, catalysis, and energy conversion. Here, we demonstrate spectrally resolved SERS imaging, to simultaneously image and collect the SERS spectra from molecules adsorbed on individual nanoparticles. We observe intensity and frequency fluctuations in the SERS signal on the time scale of tens of milliseconds from *n*-mercaptobenzoic acid (MBA) adsorbed to gold nanoparticles. The SERS signal fluctuations correlate with density functional theory calculations of radicals generated by the interaction between MBA and plasmon-generated hot electrons. Applying localization microscopy to the data provides a super-resolution spectrally resolved map that indicates the plasmonic-induced molecular charging occurs on the extremities of the nanoparticles, where the localized electromagnetic field is reported to be most intense.

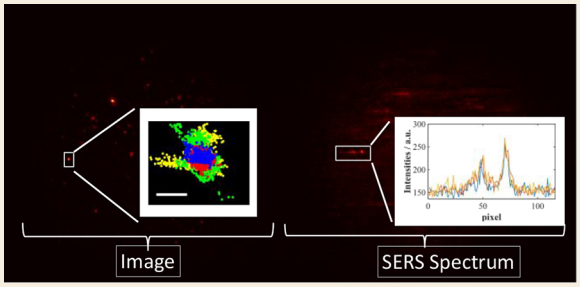

KEYWORDS: *SERS, plasmonics, super-resolution, electron transfer, nanoparticles, Raman, spectroscopy, microscopy*

The ability to concentrate light and induce energetic charge carriers by nanoparticles with plasmon resonances has enabled new avenues of research in diverse applications.[1] When light of the appropriate energy is incident on metallic surfaces, a collective oscillation of the conduction band electrons generates what is known as a plasmon or more specifically as a localized surface-plasmon resonance (LSPR) in plasmonic nanoparticles. The electromagnetic fields generated on the nanoparticle surface are orders of magnitude larger than the incident light. Molecules within the enhanced field can experience different chemical and physical behaviors, such as optical signal enhancement,[2] optical trapping,[3] molecular charging,[4] optical rectification,[4,5] and chemical conversion.[6] Understanding and controlling molecules coupled to these plasmonic systems is the key to improve the efficiency of solar cells,[7] generate energetic charge carriers as a precursor of chemical reactions in catalysis,[8−10] induce surface potentials in nanogaps,[4,9] achieve high-sensitivity sensing,[2] and image with atomic resolution in tip-enhanced Raman.[11] Novel approaches combining spectroscopy and imaging that reveal the nature of the nanomaterial−molecule interaction will be fundamental in elucidating plasmon-mediated mechanisms and developing next-generation materials.

Much of the current understanding of plasmonic effects comes from the efforts concentrated on the correlations between light and nanostructured materials.[12,13] A number of experimental geometries, such as nanogaps,[14,15] tips,[16] nanoparticle-on-mirror,[17] and nanoshells,[18] have been explored and shown to generate extraordinary optical responses. In general, there has been parallel development of theory and experiment to elucidate the properties observed.[18−22] While significant work has been reported for understanding the behavior of the electric fields on nanoparticles, understanding of the molecular response in these peculiar localized electromagnetic fields has been more limited.

The understanding of the molecular response has benefitted from work in plasmonic catalysis, which is based on the transfer of electrons between molecules and plasmonic materials. One of the first reports illustrated how H_2 gas could be dissociated on gold nanoparticles when the plasmon resonance was excited.[23] This has led to an increasing number of reports illustrating how the electrons and electric fields associated with plasmon resonances can be captured for chemical conversion.[6,13,24] Additional work has addressed the relative contributions of hot electrons versus thermalized electrons that arise from plasmon excitation, helping understanding of the mechanisms driving reactivity on the nanoparticle.[25]

Received: September 18, 2021
Revised: October 26, 2021
Accepted: October 28, 2021
Published: December 1, 2021

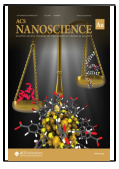

https://doi.org/10.1021/acsnanoscienceau.1c00031
ACS Nanosci. Au 2021, 1, 38–46

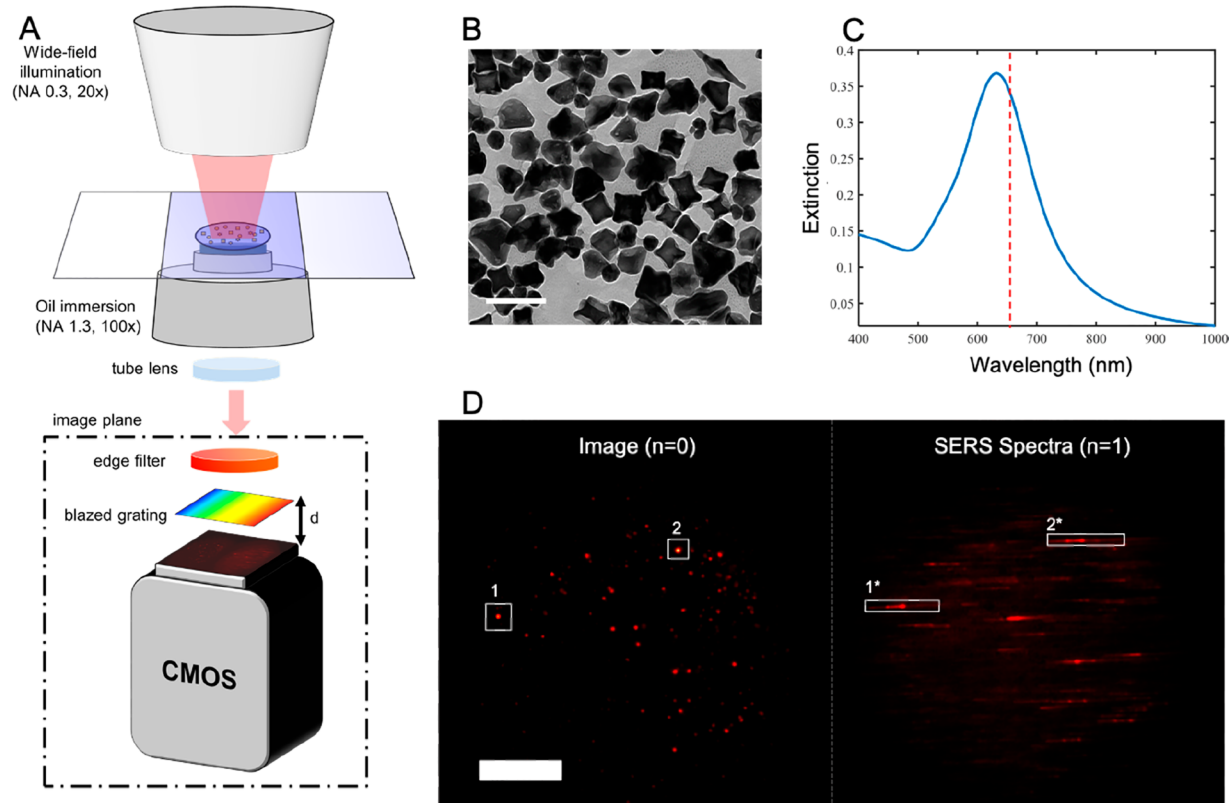

Figure 1. Spectrally resolved SERS setup. (A) The schematic for the spectrally resolved SERS imaging of nanoparticles in solution is shown. SERS signals (image and spectra) are collected in transmission mode, using a 659 nm laser, two objectives (top: wide-field illumination, NA 0.3, 20×; bottom: collection, oil immersion, NA 1.3, 100×), tube lens, edge filter (Semrock, 660 nm), transmission grating (300 grooves/nm), and a two-dimensional complementary metal oxide semiconductor camera (2D-CMOS, ORCA-Flash 4.0 V3, Hamamatsu). (B) The TEM image of the synthesized nanoparticles used in this work is shown, where the scale bar is 150 nm. The nanoparticles exhibit branches that generate large plasmonic "hotspots" essential to support the confined, high-intensity electromagnetic fields on their surface. (C) The ensemble extinction spectra for the nanoparticles in solution are shown. The localized surface-plasmon resonance (LSPR) peak for the ensemble measurement was observed near 640 nm. The excitation laser for SERS is noted with the vertical red dashed line. (D) A typical spatial image (zeroth-order diffraction) and SERS spectra (first-order diffraction) signals recorded on the camera sensor for individual nanoparticles simultaneously. Particles 1 and 2 discussed in the text are noted with their respective spectra. The scale bar is 10 μm.

Several mechanisms have been put forth to explain the catalytic activity on plasmonic particles. Chemical interface dampening suggests molecules at the surface influence the dephasing of the excited plasmon resonance, which results in increased photon absorption relative to scattering and opens new pathways for electron transfer.[26] Plasmon-induced resonant energy transfer was put forth to explain the transfer of electrons from metal nanoparticles to semiconductors,[27] where spectral overlap between the metal plasmon and the semiconductor absorption increases the charge density of the semiconductor.[28] The increase in charge density can displace the Fermi level[29] and thereby increase the energy of the electrons present on the metal surface for catalysis. Another recent report postulated that electrochemically active molecules in solution consume photo-excited electrons/holes, causing a buildup of the remaining charge that alters the surface potential and influences the reactivity of the plasmonic particles.[9] This change in surface potential was incorporated into formalism derived from the Nernst equation, illustrating the change in overpotential for many reactions.[30] A common element in all these theories is the interaction of molecules with the plasmon resonance, thus illustrating important processes occurring.

A key challenge to investigating the molecular response on plasmonic materials is the chemical sensitivity and temporal resolution of the measurement. It has been reported that electron transfer in plasmonic systems can be monitored by the species observed in surface-enhanced Raman scattering (SERS) measurements.[31,32] Protein fragmentation is observed when high-energy electrons are captured in tip-enhanced Raman scattering (TERS) experiments.[31] Alternatively, the formation of longer-lived radical species has been reported in SERS experiments with proteins.[32] There have also been reports of electron capture to form anion species in other molecules, which were detected by changes in the observed SERS spectrum.[24,33−35] The SERS spectrum is known to be dominated by long-lived species, which can wash out the signal from transient intermediates,[36] which requires measurements with rapid signal collection to capture and characterize transient species on the plasmonic particles.

Here, we investigate spectrally resolved SERS imaging for monitoring plasmon-mediated chemical transformations from individual nanoparticles in solution. SERS intensity fluctuations (SIFs) are commonly observed in the SERS signal from individual nanoparticles.[37] In spectrally resolved SERS imaging, the SIFs from single nanoparticles are rapidly imaged (10 Hz) on a two-dimensional complementary metal oxide semiconductor (2D-CMOS) camera, similar to imaging demonstrated in previous approaches.[38] However, rather than integrating the total intensity of SIFs from a spectral range,[39−41] in spectrally resolved SERS imaging, the position

https://doi.org/10.1021/acsnanoscienceau.1c00031
ACS Nanosci. Au 2021, 1, 38−46

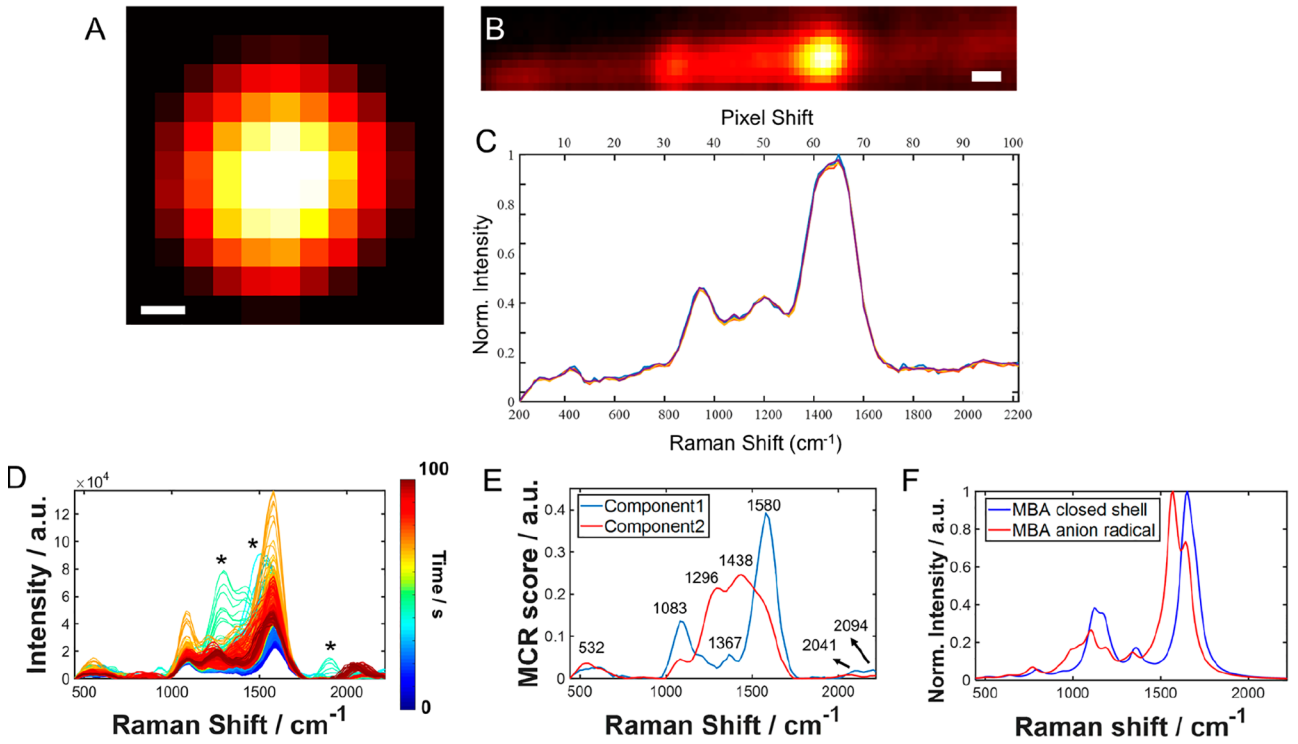

Figure 2. Spectrally resolved SERS imaging recorded at 10 Hz. (A) Spatial (n = 0) and (B) spectral (n = 1) signals from the diffraction grating are shown for particle #1 in Figure 1D. In the spatial dimension (A), each pixel is 60 nm. The spectral dispersion in (B) is approximately 1 nm (18 cm^{-1} Raman shift) per pixel. (C) The spectra are shown by averaging 10 adjacent pixels in the y-direction from the n = 1 signal of four single camera frames. The first frame shows clear peaks at pixels 37 and 65, which correspond to 1580 and 1083 cm^{-1} Raman shifts, which are observed in most of the other frames. (D) The time-evolved spectra are plotted after calibration of the x-axis. The asterisk indicate the transient vibrational modes. (E) The two SERS components determined by MCR analysis shown explain 97% of the variance in the spectra. (F) The simulated Raman spectra of MBA and the MBA with an extra electron are shown using CAM-B3LYP/6-31+G(d). The simulated spectra are broadened with a line width of 40 cm^{-1} and scaled by 0.94 to match the symmetric ring stretch of the closed-shell species with the experimentally observed peak at 1580 cm^{-1}. The scale bars are (A) 100 nm and (B) 100 cm^{-1}.

and SERS spectrum associated with the intensity fluctuation are recorded on the same camera sensor (Figure 1, see also Supporting Information). This approach, also called snapshot spectral imaging, has been previously demonstrated in fluorescence[42] and dark-field electronic scattering.[43] Here, we extend this approach to monitor the vibrational structure captured in the SERS spectrum. Moreover, the transient nature of SIFs enables localization algorithms[44] to be applied and generates a super-resolution SERS spectral map. In this report, we use this approach to study and identify the chemical origins of signal fluctuations of nanoparticles on the nanometer scale.

RESULTS AND DISCUSSION

Figure 1 illustrates our experiment. Figure 1A diagrams the custom instrument, incorporating an inverted microscope with wide-field laser illumination of the sample from a top objective (NA 0.3, 20×) and image and signal collection through the microscope objective (oil immersion, NA 1.3, 100×). Using two independent objectives enables the laser spot size to be adjusted by changing the distance between the top objective and sample while keeping the sample in focus without further changes in the position. This effectively allows us to mask part of the field of view (FoV) and only collect the SERS signal from the selected area ~30 μm across, with a power density of 1.5 kW cm^{-2}. Under these conditions, we observe large intensity fluctuations from individual nanoparticles above a baseline signal intensity of 5.5 × 10^5 photons s^{-1} (Figure S1). The sample consists of asymmetric nanoparticles; the transmission electron microscopy (TEM) and ensemble extinction spectrum are shown in Figure 1B,C, respectively. The Rayleigh scattering, anti-Stokes scattering, and other spurious emissions were removed by using a long-pass filter, allowing only SERS photons to reach the detector. Previous work has demonstrated that a low luminescence and/or fluorescence signal can still pass through the filter; however, this background can be easily neglected relative to the higher-intensity SERS signal.[40,44] Finally, a transmission diffraction grating is placed between the edge filter and the 2D-CMOS sensor. The image plane recorded by the detector simultaneously captures both the zeroth-order diffraction (spatial image) and the first-order diffraction (spectrum) from each point in the FoV (Figure 1D). Optimization of the distance, d (ca. 20 mm), between the blazed grating and camera sensor avoids overlap between the zeroth- and first-order signals and determines the spectral resolution (Figure S2). The observed dispersion is 1.1 nm/pixel, which agrees with the calculated dispersion of 1.02 nm/pixel for the 300 groove/mm grating and separation distance (d) used.

Spectrally Resolved SERS Imaging

Using this approach, we simultaneously recorded the spatial position and SERS spectra of several single nanoparticles in solution (Figure 1D). Using the grating to capture the SERS spectrum concurrently with the image on the same sensor eliminates the need for a second spectrometer or camera used in other work.[38,39] Figure 2 shows data collected at a 10 Hz frame rate from a selected nanoparticle in the spectrally resolved SERS

https://doi.org/10.1021/acsnanoscienceau.1c00031
ACS Nanosci. Au 2021, 1, 38−46

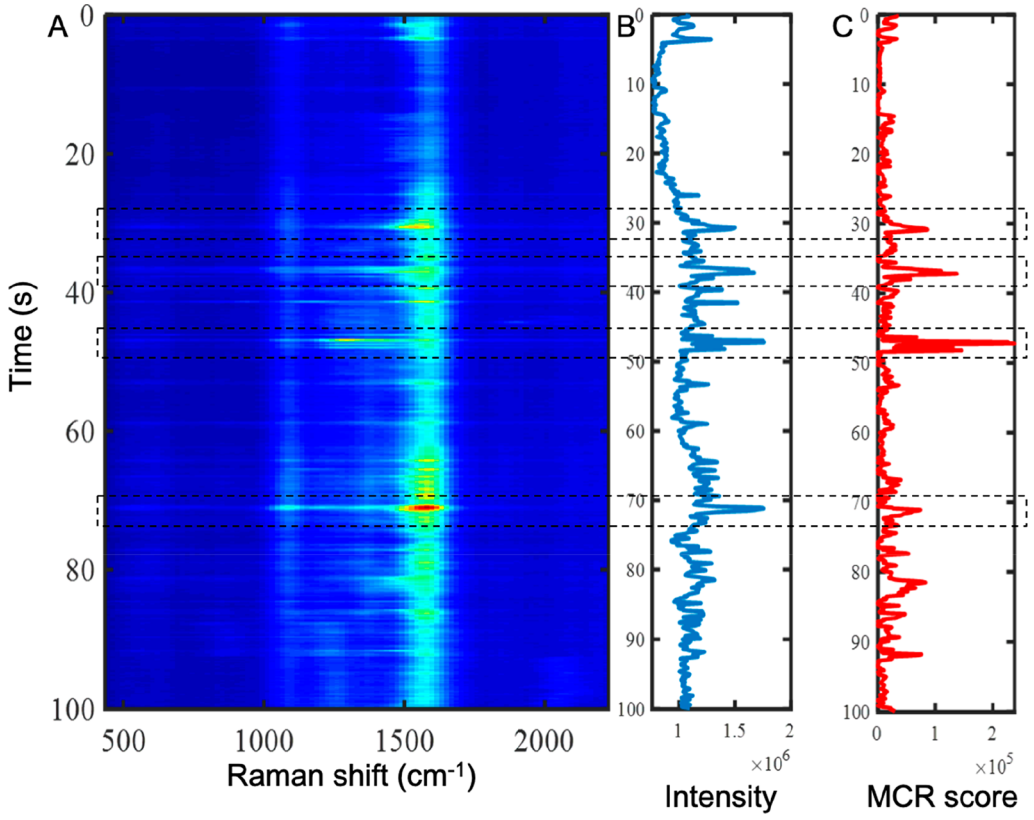

Figure 3. SERS time evolution analysis. Time trajectories for (A) spectra, (B) integrated intensities, and (C) MCR scores for component 2. The arrows indicate that some of the most intense SIFs were highly correlated in time with the recovered spectrum in Figure 2E (red line), which could explain the origin of these fluctuations in the SERS signal.

image (particle 1, Figure 1D), where both the position and SERS spectra were recorded simultaneously (Figure 2A,B). The emission from the particle has spherical symmetry (Figure 2A) and the full width at half-maximum (fwhm) is 340 nm, both of which suggest that a single nanoparticle is being imaged.[38,44] The fwhm is consistent with the diffraction-limited spot of approximately 300 nm in our setup (Figure S3). Applying localization methods, we generate a super-resolution image of the nanoparticle with a size of 100 nm (Figure S4A), consistent with the TEM results in Figure 1B.

Examining the wavelength-dispersed signal from the diffraction grating, a clear SERS spectrum is observed. The spectral dispersion can be calibrated to convert the spacing along the sensor array into units of energy (Figure S2). The spectral resolution is estimated to be ~18 cm^{-1}/pixel across the Raman spectrum, which is reasonable when compared with calibration data (Figure S2). Using localization algorithms on the spectral band of 1580 cm^{-1} (Figure S4C,D), the center of the band varies by 40 cm^{-1} in the spectral domain, suggesting changes in the emission location blur the observed spectral resolution. The spectral domain exhibits very intense SERS spectra, and strong bands attributable to the MBA adsorbed on the nanoparticle surface are observed at 1580 and 1083 cm^{-1} (Figure 2B,C).[45,46] To account for a small angular deviation in the wavelength-dispersed signal, we integrated 10 adjacent pixels in the *y*-direction. Figure 2C shows the SERS spectra from the selected particle generated by integrating the first four frames collected.

Dynamic SERS Imaging

Figure 2D shows time-dependent SERS spectra of particle 1 highlighted in Figure 1 recorded for 100 s at 10 Hz. Interestingly, we observe a dynamic spectrum, as opposed to the spectrum recorded from ensemble averaging for an extended period or the spectrum recorded from MBA in the ensemble solution (Figures 2D and S5, respectively). The steady-state spectrum and the ensemble spectrum largely consist of the prominent ring-breathing modes from the aromatic ring in the MBA molecule at 1083 and 1580 cm^{-1} (Figure S5). In fact, SIFs were frequent and consistent over the period of a few minutes. By resolving the frequencies contained in the SIFs, changes in the measured vibrational bands are clearly observed (Figure 2D), consistent with prior reports.[37,39,47] However, the appearance and disappearance of bands in the vibrational spectrum indicated by the asterisk in Figure 2D are observed over the acquisition period, suggesting molecular changes are occurring. These changes require resolving the spectrum to observe and are lost when only the intensity is monitored.

To facilitate the interpretation of these dynamics, the recorded spectra were decomposed using multivariate curve resolution (MCR) analysis to identify spectral changes in time. The results show that two main components successfully recover over 97% of variance contained in the time-dependent spectra (Figure 2E). The first component shows vibrational bands at 1083 and 1580 cm^{-1}, which is consistent with the ensemble average SERS spectrum of MBA. Component 2 shows significant vibrational bands at 1296 and 1438 cm^{-1}. Component 2 is observed in short bursts and averages into the background over extended signal acquisitions, consistent with the observation of rare events in SERS.[36]

Previous reports have shown that energetic charge carriers can impact the SERS spectrum of molecules on plasmonic nanoparticles. As noted above, electron capture can yield

https://doi.org/10.1021/acsnanoscienceau.1c00031
ACS Nanosci. Au 2021, 1, 38−46

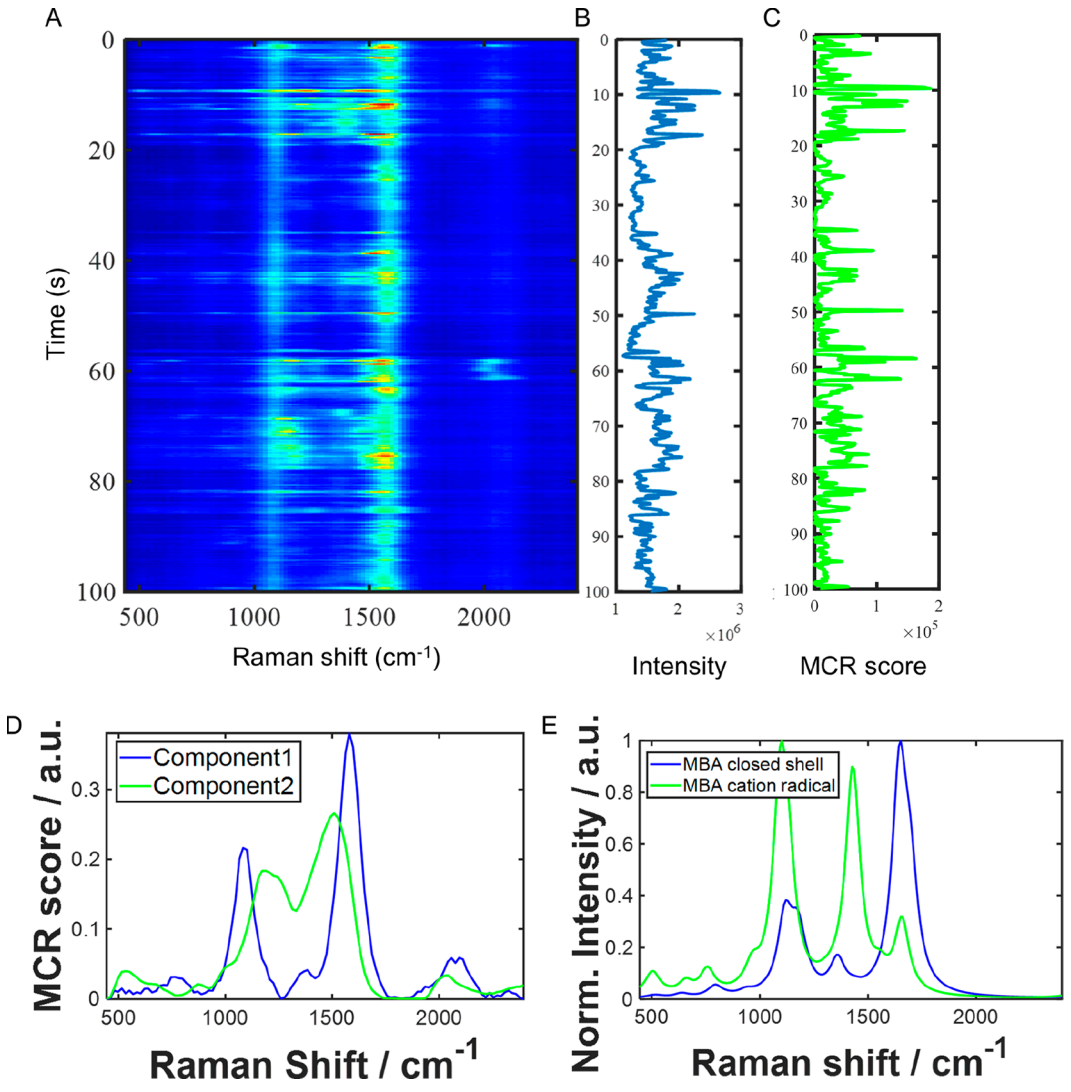

Figure 4. Spectral fluctuations suggesting alternate photoproducts. (A) The time-varying SERS spectra observed from particle 2 (Figure 1) are shown along with the (B) the total intensity fluctuations and (C) the MCR scores for component 2. (D) Decomposition of the SERS signal by MCR reveals two components, component 1 (blue), which is consistent with the closed-shell MBA spectrum, and component 2 (green), which is observed during intense signal fluctuations. (E) CAM-B3LYP/6-31+G(d)-simulated spectra indicate the spectral shifts in component 2 may be explained by the formation of the MBA cation radical (green).

radicals, trigger redox processes, and generate molecular fragments in plasmonic systems.[4,24,31,33,43] Of particular interest was the report that radicals can exhibit increased Raman scattering.[32]

To examine this hypothesis, density functional theory (DFT) calculations were performed on the MBA absorbate. Figure 2E,F compares the experimentally determined MCR components with the CAM-B3LYP/6-31+G(d)-simulated spectra of MBA and the MBA anion radical. The simulated spectra have been broadened to match the experimental resolution, using a 40 cm^{-1} line width. The calculated Raman frequencies were scaled by 0.94, determined by matching the experimental (1580 cm^{-1}) and calculated symmetric ring stretch in the closed-shell MBA molecule. The same scaling and line broadening were then applied to the radical species calculated at the same level of theory. Of particular note, the simulated closed-shell Raman spectrum of MBA in Figure 2F shows excellent agreement with component 1 and indicates this component arises from SERS of MBA at the surface of the particles. Upon electron capture to form the MBA anion radical, the symmetric ring stretch is calculated to shift to lower energy, which accounts for the experimental band at 1438 cm^{-1}. There is strong qualitative agreement between experimentally observed frequency shifts in component 2 and the simulated spectrum of the anion radical. The transient formation of the anion radical provides a molecular explanation for the observed changes in the SERS spectrum. The band observed at 1299 cm^{-1} correlates well with the ring mode in the calculation at 1283 cm^{-1}. The difference in intensity may arise from an element of resonance enhancement associated with adsorbed aromatic thiols not included in our model.

Figure 3 compares the spectral fluctuations (Figure 3A) with overall signal intensity versus time of the nanoparticle (Figure 3B) and the time trajectory associated with component 2 determined from the MCR analysis (Figure 3C). Well-resolved spectra are denoted by the dashed boxes in Figure 3A that correlate with highest signal intensities marked with dashed boxes in Figure 3B. Moreover, component 2, attributed to the anion radical, correlates with the short-time and very intense SIFs (Figure 3B,C, indicated by the dashed boxes), which

https://doi.org/10.1021/acsnanoscienceau.1c00031
ACS Nanosci. Au 2021, 1, 38−46

suggests the transient formation of this anion radical may give rise to the SIFs observed from the nanoparticle. The acquisition time shown in Figure 3 is 100 ms per frame, and most fluctuations appear to persist for a single frame, suggesting the radical species is stable for 10s to 100s of milliseconds (Figure S6). This lifetime is consistent with single-molecule fluorescence measurements reported on Au nanorods that showed photo-induced electron transfer generated blinking on similar time scales.[48] A clear advantage in our current work is that nonfluorescent molecules can also be studied.

By monitoring the Raman signal from different particles, we observe many particles that behave like particle 1 discussed above (see Supplementary Video 1). We also observe a subset of particles that exhibit a different time-fluctuating Raman response. Figure 4 shows the time-varying SERS signal observed from "particle 2" observed in Figure 1. MCR analysis again extracts component 1, which is consistent with closed-shell MBA adsorbed to the nanoparticles. Like particle 1, intense spectra (Figure 4A) correlate with overall scattering intensity (Figure 4B) and the MCR score for component 2. However, component 2 now shows a different spectral response with significant bands at 1189 and 1509 cm^{-1} (Figure 4D). It is reported that excitation on either side of the LSPR can promote electron transfer to (for excitation wavelengths less than the LSPR) or from (for excitation wavelengths greater than the LSPR) the irradiated nanoparticle.[49] From the TEM image (Figure 1), we see that our nanoparticles are relatively heterogeneous in size and shape, which should exhibit LPSRs on both sides of our laser frequency (659 nm). We again performed DFT calculations to assess if the MBA cation radical could be responsible for this second behavior. The DFT calculations for cation radical again show a shift in the ring modes and some qualitative agreement with the experimentally derived MCR component 2, suggesting a molecular explanation for the differences observed. Inspection of the spectra in Figure 4A and the derived MCR components (Figure 4D) show other features that might also be explained by chemical conversion, or fragmentation, occurring on the nanoparticle surface.

Super-resolution Spectrally Resolved SERS Mapping

To further explore the connection between the plasmon resonance and the observed molecular behavior, we applied super-resolution SERS analysis[38,44] to track the emission based on the peaks observed in the spectral response (Figure 5). The SIF evolution in time can be used to localize the position of the emitter on the nanoparticle within the diffraction-limited spot by using super-resolution SERS fitting.[40,44] Plotting the emission centroid for time points with vibrational bands around 1083 cm^{-1} (blue dots) and 1580 cm^{-1} (red dots), attributed to the closed-shell MBA species, and 1296 cm^{-1} (green dots) and 1438 cm^{-1} (yellow dots), attributed to the anion radical, we see a marked difference in the spatial origin of the signals (Figure 5A). Examining the time trajectories for each SERS band (Figure 5B), the bands at 1083 and 1580 cm^{-1} correlate well (R^2 = 0.95), as do the bands at 1438 and 1296 cm^{-1} (R^2 = 0.85). Here, the super-resolved image provides nanoscale spatial information about the chemical transformations. For example, the bands attributed to the anion radical appear on the extremities, while the closed-shell species is observed toward the center of the particle. This spatially localized anion formation is consistent with prior work showing oxidation and reduction occurring at spatially distinct points on nanoparticles.[50] It is known that the electric fields are strongest at the points of these asymmetric

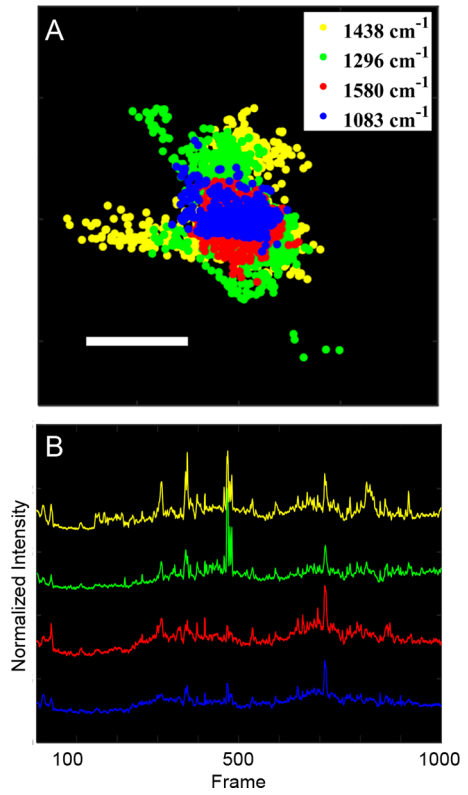

Figure 5. Colocalization of the frequencies observed in SIFs from a single nanoparticle. (A) Applying localization algorithms to the collected spectral data generates a super-resolution image of the emission from a single nanoparticle. The frequencies correlated with the anion radical spectrum are observed to locate at extremities consistent with (B) time trajectory for the vibrational modes, where good correlation was observed between modes at 1580 and 1083 cm^{-1} (R^2 = 0.95) and 1438 and 1296 cm^{-1} (R^2 = 0.85). Note: The TEM image of the nanoparticles used is shown on Figure 1B. The scale bar in (A) is 20 nm.

particles and seem to be active sites of electron transfer. At the coverage of molecules used, the emission will localize to an intensity-weighted position representative of all the radiating molecules on the nanoparticle.[51] The intensity-weighted superposition may cause the super-resolved image (Figure 5A) to appear smaller than the particles in the TEM image.

Current theories regarding the SIFs at a single-nanoparticle level implicate the surface roughness of the single nanoparticle formed by protrusions and adatoms.[37,40,52] These atomic dislocations have been called "picocavities",[53] which support highly confined intense electromagnetic fields in very small volumes.[54] It has been suggested that these intense fields can generate strong plasmonic enhancement effects that alter the symmetry of adsorbed molecules, altering the observed spectrum.[55−57] The observation of electron transfer at the points of the nanoparticles used here is consistent with the importance of the strong electric fields; however, our results indicate that metastable electron-transfer species correlate with the spectroscopic changes. We also note that our spectra also show low-intensity features between 2000−2100 cm^{-1} and near 1900 cm^{-1}, which may represent other photoproducts in our experiments. The vibrational signal may also arise from faster dynamics associated with nanoparticle adatom reorganization or other effects. Additional work is needed to address the

https://doi.org/10.1021/acsnanoscienceau.1c00031
ACS Nanosci. Au 2021, 1, 38−46

mechanisms and stability of other processes occurring in these systems.

CONCLUSION

In conclusion, we have demonstrated that a time-varying SERS spectral response indicates the formation of electron-transfer species occurring on the surface of gold nanoparticles in solution. Spectral SERS imaging is capable of simultaneous super-resolution imaging and spatially resolved spectroscopy. The observed spectral changes are consistent with DFT calculations of anion and cation radical species. The duration of the signal fluctuations is consistent with charge transfer events previously reported using single-molecule fluorescence imaging; however, the use of the SERS signal enables us to determine the chemical transformations that occur in a nonfluorescent molecule. Further, our data strongly indicates that molecular species on the nanoparticle surface contribute to SIFs, providing strong evidence for the importance of considering the specific molecules and their behavior on plasmonic particles.

ASSOCIATED CONTENT

Supporting Information

The Supporting Information is available free of charge at https://pubs.acs.org/doi/10.1021/acsnanoscienceau.1c00031.

Experimental methods and Figures S1−S5 describing calibration and sample characterization (PDF)

Supplementary Video 1: Monitoring the observed Raman signal from different particles in a field of view (MP4)

AUTHOR INFORMATION

Corresponding Author

Zachary D. Schultz − *Department of Chemistry and Biochemistry, The Ohio State University, Columbus, Ohio 43210, United States;* orcid.org/0000-0003-1741-8801; Email: Schultz.133@osu.edu

Authors

Carlos Diego L. de Albuquerque − *Department of Chemistry and Biochemistry, The Ohio State University, Columbus, Ohio 43210, United States;* Present Address: CIC biomaGUNE, Basque Research and Technology Alliance (BRTA), 20014 San Sebastián, Spain. (C.D.L.d.A.); orcid.org/0000-0002-7615-7325

Chelsea M. Zoltowski − *Department of Chemistry and Biochemistry, The Ohio State University, Columbus, Ohio 43210, United States*

Brian T. Scarpitti − *Department of Chemistry and Biochemistry, The Ohio State University, Columbus, Ohio 43210, United States*

Deben N. Shoup − *Department of Chemistry and Biochemistry, The Ohio State University, Columbus, Ohio 43210, United States*

Complete contact information is available at: https://pubs.acs.org/10.1021/acsnanoscienceau.1c00031

Author Contributions

C.D.L.d.A. designed and carried out the experiments as well as analyzed and interpreted results. C.M.Z. carried out the simulations. B.T.S. synthesized and characterized the nanoparticles. D.N.S. performed calibration experiments. Z.D.S. conceived of and supervised the project as well as analyzed and interpreted the results. Z.D.S. and C.D.L.d.A. wrote the manuscript with contributions from the other authors.

Notes

The authors declare no competing financial interest.

ACKNOWLEDGMENTS

The work was supported by the Ohio State University, the Ohio State Comprehensive Cancer Center through NIH award P30 CA016058, and NIH award R01 GM109988. Calculations were performed through the Ohio Supercomputer Center.

REFERENCES

(1) Halas, N. J.; Lal, S.; Chang, W. S.; Link, S.; Nordlander, P. Plasmons in Strongly Coupled Metallic Nanostructures. *Chem. Rev.* **2011**, *111* (6), 3913−3961.

(2) Langer, J.; Jimenez de Aberasturi, D.; Aizpurua, J.; Alvarez-Puebla, R. A.; Auguié, B.; Baumberg, J. J.; Bazan, G. C.; Bell, S. E. J.; Boisen, A.; Brolo, A. G.; Choo, J.; Cialla-May, D.; Deckert, V.; Fabris, L.; Faulds, K.; García de Abajo, F. J.; Goodacre, R.; Graham, D.; Haes, A. J.; Haynes, C. L.; Huck, C.; Itoh, T.; Käll, M.; Kneipp, J.; Kotov, N. A.; Kuang, H.; Le Ru, E. C.; Lee, H. K.; Li, J.-F.; Ling, X. Y.; Maier, S. A.; Mayerhöfer, T.; Moskovits, M.; Murakoshi, K.; Nam, J.-M.; Nie, S.; Ozaki, Y.; Pastoriza-Santos, I.; Perez-Juste, J.; Popp, J.; Pucci, A.; Reich, S.; Ren, B.; Schatz, G. C.; Shegai, T.; Schlücker, S.; Tay, L.-L.; Thomas, K. G.; Tian, Z.-Q.; Van Duyne, R. P.; Vo-Dinh, T.; Wang, Y.; Willets, K. A.; Xu, C.; Xu, H.; Xu, Y.; Yamamoto, Y. S.; Zhao, B.; Liz-Marzán, L. M. Present and Future of Surface-Enhanced Raman Scattering. *ACS Nano* **2020**, *14* (1), 28−117.

(3) Juan, M. L.; Righini, M.; Quidant, R. Plasmon nano-optical tweezers. *Nat. Photonics* **2011**, *5* (6), 349−356.

(4) El-Khoury, P. Z.; Schultz, Z. D. From SERS to TERS and Beyond: Molecules as Probes of Nanoscopic Optical Fields. *J. Phys. Chem. C* **2020**, *124* (50), 27267−27275.

(5) Ward, D. R.; Huser, F.; Pauly, F.; Cuevas, J. C.; Natelson, D. Optical rectification and field enhancement in a plasmonic nanogap. *Nat. Nanotechnol.* **2010**, *5* (10), 732−6.

(6) Zhang, Y. C.; He, S.; Guo, W. X.; Hu, Y.; Huang, J. W.; Mulcahy, J. R.; Wei, W. D. Surface-Plasmon-Driven Hot Electron Photochemistry. *Chem. Rev.* **2018**, *118* (6), 2927−2954.

(7) Jang, Y. H.; Jang, Y. J.; Kim, S.; Quan, L. N.; Chung, K.; Kim, D. H. Plasmonic Solar Cells: From Rational Design to Mechanism Overview. *Chem. Rev.* **2016**, *116* (24), 14982−15034.

(8) Verma, R.; Belgamwar, R.; Polshettiwar, V. Plasmonic Photocatalysis for CO2 Conversion to Chemicals and Fuels. *ACS Materials Letters* **2021**, *3* (5), 574−598.

(9) Wilson, A. J.; Jain, P. K. Light-Induced Voltages in Catalysis by Plasmonic Nanostructures. *Acc. Chem. Res.* **2020**, *53* (9), 1773−1781.

(10) Cortés, E.; Besteiro, L. V.; Alabastri, A.; Baldi, A.; Tagliabue, G.; Demetriadou, A.; Narang, P. Challenges in Plasmonic Catalysis. *ACS Nano* **2020**, *14* (12), 16202−16219.

(11) Kurouski, D.; Dazzi, A.; Zenobi, R.; Centrone, A. Infrared and Raman chemical imaging and spectroscopy at the nanoscale. *Chem. Soc. Rev.* **2020**, *49* (11), 3315−3347.

(12) Hartland, G. V. Optical Studies of Dynamics in Noble Metal Nanostructures. *Chem. Rev.* **2011**, *111* (6), 3858−3887.

(13) Brongersma, M. L.; Halas, N. J.; Nordlander, P. Plasmon-induced hot carrier science and technology. *Nat. Nanotechnol.* **2015**, *10* (1), 25−34.

(14) Alexander, K. D.; Skinner, K.; Zhang, S. P.; Wei, H.; Lopez, R. Tunable SERS in Gold Nanorod Dimers through Strain Control on an Elastomeric Substrate. *Nano Lett.* **2010**, *10* (11), 4488−4493.

(15) Wustholz, K. L.; Henry, A.-I.; McMahon, J. M.; Freeman, R. G.; Valley, N.; Piotti, M. E.; Natan, M. J.; Schatz, G. C.; Van Duyne, R. P. Structure-Activity Relationships in Gold Nanoparticle Dimers and Trimers for Surface-Enhanced Raman Spectroscopy. *J. Am. Chem. Soc.* **2010**, *132* (31), 10903−10910.

(16) Deckert-Gaudig, T.; Taguchi, A.; Kawata, S.; Deckert, V. Tip-enhanced Raman spectroscopy - from early developments to recent advances. *Chem. Soc. Rev.* **2017**, *46* (13), 4077−4110.
(17) Chikkaraddy, R.; de Nijs, B.; Benz, F.; Barrow, S. J.; Scherman, O. A.; Rosta, E.; Demetriadou, A.; Fox, P.; Hess, O.; Baumberg, J. J. Single-molecule strong coupling at room temperature in plasmonic nanocavities. *Nature* **2016**, *535* (7610), 127−130.
(18) Prodan, E.; Radloff, C.; Halas, N. J.; Nordlander, P. A Hybridization Model for the Plasmon Response of Complex Nanostructures. *Science* **2003**, *302* (5644), 419−422.
(19) Haynes, C. L.; Van Duyne, R. P. Nanosphere lithography: A versatile nanofabrication tool for studies of size-dependent nanoparticle optics. *J. Phys. Chem. B* **2001**, *105* (24), 5599−5611.
(20) Jensen, T. R.; Malinsky, M. D.; Haynes, C. L.; Van Duyne, R. P. Nanosphere lithography: Tunable localized surface plasmon resonance spectra of silver nanoparticles. *J. Phys. Chem. B* **2000**, *104* (45), 10549−10556.
(21) Zuloaga, J.; Prodan, E.; Nordlander, P. Quantum Description of the Plasmon Resonances of a Nanoparticle Dimer. *Nano Lett.* **2009**, *9* (2), 887−891.
(22) Wang, D. S.; Kerker, M. Enhanced Raman-Scattering by Molecules Adsorbed at the Surface of Colloidal Spheroids. *Phys. Rev. B: Condens. Matter Mater. Phys.* **1981**, *24* (4), 1777−1790.
(23) Mukherjee, S.; Libisch, F.; Large, N.; Neumann, O.; Brown, L. V.; Cheng, J.; Lassiter, J. B.; Carter, E. A.; Nordlander, P.; Halas, N. J. Hot Electrons Do the Impossible: Plasmon-Induced Dissociation of H2 on Au. *Nano Lett.* **2013**, *13* (1), 240−247.
(24) Yin, H.; Lan, J.-G.; Goubert, G.; Wang, Y.-H.; Li, J.-F.; Zenobi, R. Nanoscale Surface Redox Chemistry Triggered by Plasmon-Generated Hot Carriers. *Small* **2019**, *15* (47), 1903674.
(25) Zhou, L.; Swearer, D. F.; Zhang, C.; Robatjazi, H.; Zhao, H.; Henderson, L.; Dong, L.; Christopher, P.; Carter, E. A.; Nordlander, P.; Halas, N. J. Quantifying hot carrier and thermal contributions in plasmonic photocatalysis. *Science* **2018**, *362* (6410), 69−72.
(26) Therrien, A. J.; Kale, M. J.; Yuan, L.; Zhang, C.; Halas, N. J.; Christopher, P. Impact of chemical interface damping on surface plasmon dephasing. *Faraday Discuss.* **2019**, *214*, 59−72.
(27) Wu, N. Plasmonic metal-semiconductor photocatalysts and photoelectrochemical cells: a review. *Nanoscale* **2018**, *10* (6), 2679−2696.
(28) Cushing, S. K.; Li, J.; Bright, J.; Yost, B. T.; Zheng, P.; Bristow, A. D.; Wu, N. Controlling Plasmon-Induced Resonance Energy Transfer and Hot Electron Injection Processes in Metal@TiO2 Core−Shell Nanoparticles. *J. Phys. Chem. C* **2015**, *119* (28), 16239−16244.
(29) Singh, A. N.; Devnani, H.; Jha, S.; Ingole, P. P. Fermi level equilibration of Ag and Au plasmonic metal nanoparticles supported on graphene oxide. *Phys. Chem. Chem. Phys.* **2018**, *20* (41), 26719−26733.
(30) Yu, S.; Jain, P. K. The Chemical Potential of Plasmonic Excitations. *Angew. Chem., Int. Ed.* **2020**, *59* (5), 2085−2088.
(31) Szczerbiński, J.; Gyr, L.; Kaeslin, J.; Zenobi, R. Plasmon-Driven Photocatalysis Leads to Products Known from E-beam and X-ray-Induced Surface Chemistry. *Nano Lett.* **2018**, *18* (11), 6740−6749.
(32) Sloan-Dennison, S.; Zoltowski, C. M.; El-Khoury, P. Z.; Schultz, Z. D. Surface Enhanced Raman Scattering Selectivity in Proteins Arises from Electron Capture and Resonant Enhancement of Radical Species. *J. Phys. Chem. C* **2020**, *124* (17), 9548−9558.
(33) Choi, H. K.; Lee, K. S.; Shin, H. H.; Kim, Z. H. Identification of the First Elementary Step in the Photocatalytic Reduction of Nitrobenzenethiols on a Metallic Surface. *J. Phys. Chem. Lett.* **2016**, *7* (20), 4099−4104.
(34) Wang, H.; Yao, K.; Parkhill, J. A.; Schultz, Z. D. Detection of electron tunneling across plasmonic nanoparticle-film junctions using nitrile vibrations. *Phys. Chem. Chem. Phys.* **2017**, *19* (8), 5786−5796.
(35) Sprague-Klein, E. A.; Negru, B.; Madison, L. R.; Coste, S. C.; Rugg, B. K.; Felts, A. M.; McAnally, M. O.; Banik, M.; Apkarian, V. A.; Wasielewski, M. R.; Ratner, M. A.; Seideman, T.; Schatz, G. C.; Van Duyne, R. P. Photoinduced Plasmon-Driven Chemistry in trans-1,2-Bis(4-pyridyl)ethylene Gold Nanosphere Oligomers. *J. Am. Chem. Soc.* **2018**, *140* (33), 10583−10592.
(36) Asiala, S. M.; Schultz, Z. D. Label-free in situ detection of individual macromolecular assemblies by surface enhanced Raman scattering. *Chem. Commun.* **2013**, *49* (39), 4340−4342.
(37) dos Santos, D. P.; Temperini, M. L. A.; Brolo, A. G. Intensity Fluctuations in Single-Molecule Surface-Enhanced Raman Scattering. *Acc. Chem. Res.* **2019**, *52* (2), 456−464.
(38) de Albuquerque, C. D. L.; Schultz, Z. D. Super-resolution Surface-Enhanced Raman Scattering Imaging of Single Particles in Cells. *Anal. Chem.* **2020**, *92* (13), 9389−9398.
(39) de Albuquerque, C. D. L.; Hokanson, K.; Thorud, S.; Sobral-Filho, R. G.; Lindquist, N. C.; Brolo, A. G. Dynamic Imaging of Multiple SERS Hotspots on Single Nanoparticles. *ACS Photonics* **2020**, *7*, 434.
(40) Lindquist, N. C.; de Albuquerque, C. D. L.; Sobral-Filho, R. G.; Paci, I.; Brolo, A. G. High-speed imaging of surface-enhanced Raman scattering fluctuations from individual nanoparticles. *Nat. Nanotechnol.* **2019**, *14* (10), 981−987.
(41) Willets, K. A. Super-resolution imaging of SERS hot spots. *Chem. Soc. Rev.* **2014**, *43* (11), 3854−3864.
(42) Bongiovanni, M. N.; Godet, J.; Horrocks, M. H.; Tosatto, L.; Carr, A. R.; Wirthensohn, D. C.; Ranasinghe, R. T.; Lee, J.-E.; Ponjavic, A.; Fritz, J. V.; Dobson, C. M.; Klenerman, D.; Lee, S. F. Multi-dimensional super-resolution imaging enables surface hydrophobicity mapping. *Nat. Commun.* **2016**, *7* (1), 13544.
(43) Al-Zubeidi, A.; Hoener, B. S.; Collins, S. S. E.; Wang, W.; Kirchner, S. R.; Hosseini Jebeli, S. A.; Joplin, A.; Chang, W.-S.; Link, S.; Landes, C. F. Hot Holes Assist Plasmonic Nanoelectrode Dissolution. *Nano Lett.* **2019**, *19* (2), 1301−1306.
(44) Willets, K. A.; Wilson, A. J.; Sundaresan, V.; Joshi, P. B. Super-Resolution Imaging and Plasmonics. *Chem. Rev.* **2017**, *117* (11), 7538−7582.
(45) Scarpitti, B. T.; Morrison, A. M.; Buyanova, M.; Schultz, Z. D. Comparison of 4-Mercaptobenzoic Acid Surface-Enhanced Raman Spectroscopy-Based Methods for pH Determination in Cells. *Appl. Spectrosc.* **2020**, *74* (11), 1423−1432.
(46) Michota, A.; Bukowska, J. Surface-enhanced Raman scattering (SERS) of 4-mercaptobenzoic acid on silver and gold substrates. *J. Raman Spectrosc.* **2003**, *34* (1), 21−25.
(47) Dieringer, J. A.; Lettan, R. B.; Scheidt, K. A.; Van Duyne, R. P. A frequency domain existence proof of single-molecule surface-enhanced Raman Spectroscopy. *J. Am. Chem. Soc.* **2007**, *129* (51), 16249−16256.
(48) Zhang, W.; Caldarola, M.; Pradhan, B.; Orrit, M. Gold Nanorod Enhanced Fluorescence Enables Single-Molecule Electrochemistry of Methylene Blue. *Angew. Chem., Int. Ed.* **2017**, *56* (13), 3566−3569.
(49) Sheldon, M. T.; van de Groep, J.; Brown, A. M.; Polman, A.; Atwater, H. A. Plasmoelectric potentials in metal nanostructures. *Science* **2014**, *346*, 828.
(50) Wilson, A. J.; Willets, K. A. Visualizing Site-Specific Redox Potentials on the Surface of Plasmonic Nanoparticle Aggregates with Superlocalization SERS Microscopy. *Nano Lett.* **2014**, *14* (2), 939−945.
(51) Titus, E. J.; Willets, K. A. Superlocalization Surface-Enhanced Raman Scattering Microscopy: Comparing Point Spread Function Models in the Ensemble and Single-Molecule Limits. *ACS Nano* **2013**, *7* (9), 8284−8294.
(52) Xomalis, A.; Chikkaraddy, R.; Oksenberg, E.; Shlesinger, I.; Huang, J.; Garnett, E. C.; Koenderink, A. F.; Baumberg, J. J. Controlling Optically Driven Atomic Migration Using Crystal-Facet Control in Plasmonic Nanocavities. *ACS Nano* **2020**, *14* (8), 10562−10568.
(53) Carnegie, C.; Griffiths, J.; de Nijs, B.; Readman, C.; Chikkaraddy, R.; Deacon, W. M.; Zhang, Y.; Szabó, I.; Rosta, E.; Aizpurua, J.; Baumberg, J. J. Room-Temperature Optical Picocavities below 1 nm3 Accessing Single-Atom Geometries. *J. Phys. Chem. Lett.* **2018**, *9* (24), 7146−7151.
(54) Esteban, R.; Aguirregabiria, G.; Borisov, A. G.; Wang, Y. M.; Nordlander, P.; Bryant, G. W.; Aizpurua, J. The Morphology of Narrow Gaps Modifies the Plasmonic Response. *ACS Photonics* **2015**, *2* (2), 295−305.

https://doi.org/10.1021/acsnanoscienceau.1c00031
ACS Nanosci. Au 2021, 1, 38−46

(55) Ojambati, O. S.; Deacon, W. M.; Chikkaraddy, R.; Readman, C.; Lin, Q.; Koczor-Benda, Z.; Rosta, E.; Scherman, O. A.; Baumberg, J. J. Breaking the Selection Rules of Spin-Forbidden Molecular Absorption in Plasmonic Nanocavities. *ACS Photonics* **2020**, *7* (9), 2337−2342.
(56) Chiang, N.; Jiang, N.; Madison, L. R.; Pozzi, E. A.; Wasielewski, M. R.; Ratner, M. A.; Hersam, M. C.; Seideman, T.; Schatz, G. C.; Van Duyne, R. P. Probing Intermolecular Vibrational Symmetry Breaking in Self-Assembled Monolayers with Ultrahigh Vacuum Tip-Enhanced Raman Spectroscopy. *J. Am. Chem. Soc.* **2017**, *139* (51), 18664−18669.
(57) Jorio, A.; Mueller, N. S.; Reich, S. Symmetry-derived selection rules for plasmon-enhanced Raman scattering. *Phys. Rev. B: Condens. Matter Mater. Phys.* **2017**, *95* (15), 155409.

https://doi.org/10.1021/acsnanoscienceau.1c00031
ACS Nanosci. Au 2021, 1, 38−46